J Solid State Electrochem (2008) 12:353–361
DOI 10.1007/s10008-007-0499-6

ORIGINAL PAPER

A novel PEO-based composite solid-state polymer electrolyte with methyl group-functionalized SBA-15 filler for rechargeable lithium batteries

Yan-Xia Jiang · Jin-Mei Xu · Quan-Chao Zhuang · Lan-Ying Jin · Shi-Gang Sun

Received: 15 January 2007 / Revised: 9 November 2007 / Accepted: 15 November 2007 / Published online: 11 January 2008

Abstract Functionalized molecular sieve SBA-15 with trimethylchlorosilane was used as an inorganic filler in a poly(ethyleneoxide) (PEO) polymer matrix to synthesize a composite solid-state polymer electrolyte (CSPE) using $LiClO_4$ as the doping salts, which is designated to be used for rechargeable lithium batteries. The methyl group-functionalized SBA-15 (^{f}SBA-15) powder possesses more hydrophobic characters than SBA-15, which improves the miscibility between the ^{f}SBA-15 filler and the PEO matrix. The interaction between the ^{f}SBA-15 and PEO polymer matrix was investigated by scanning electron microscopy, X-ray diffraction, and differential scanning calorimetry. Linear sweep voltammetry and electrochemical impedance spectroscopy were employed to study the electrochemical stability windows, ionic conductivity, and interfacial stability of the CSPE. The temperature dependence of the change of the PEO polymer matrix in the CSPE from crystallization to amorphous phase was surveyed, for the first time, at different temperature by Fourier transform infrared emission spectroscopy. It has demonstrated that the addition of the ^{f}SBA-15 filler has improved significantly the electrochemical compatibility of the CSPE with a lithium metal electrode and enhanced effectively the ion conductivity of the CSPE.

Keywords Rechargeable lithium batteries · Composite solid-state polymer electrolyte · PEO · SBA-15 · Interfacial stability

Dedicated to Professor Oleg Petrii on the occasion of his 70th birthday on August 24th, 2007.

Y.-X. Jiang (✉) · J.-M. Xu · Q.-C. Zhuang · L.-Y. Jin · S.-G. Sun (✉)
State Key Laboratory of Physical Chemistry of Solid Surfaces, Department of Chemistry, College of Chemistry and Chemical Engineering, Xiamen University,
Xiamen 361005, China
e-mail: yxjiang@xmu.edu.cn
e-mail: sgsun@xmu.edu.cn

Introduction

The safety issue of the Li battery is vital in the development of this importance power source technology. To solve this problem caused mainly by the formation of lithium dendrites during charge/discharge in a liquid electrolyte Li-metal battery, extensive efforts have been made in which either the electrolyte or the negative electrode was modified [1]. One of approaches involves the replacing the liquid electrolyte by a dry polymer electrolyte, leading to the so-called Li solid polymer electrolyte batteries. Since Wright [2, 3] and Armand [4] reported that some polyether-based polymers incorporated with alkali metal salts exhibit ionic conductivity, the polyether-based solid polymer electrolytes have received extensive attentions. The dominating transport of Li^+ cations in the polymer electrolyte is coupled with the local relaxation and segmental motion of the poly(ethyleneoxide) (PEO) chains, which correlated with the amorphous state of the PEO. However, the polyether-based polymers that have a high crystallinity at ambient temperature yield often a very low ionic conductivity (~10^{-7} S cm^{-1}) for PEO-based polymer electrolytes. Nowadays, the polymer electrolytes are restricted to large systems (electric traction or backup power) and not to portable devices, as it operates at a temperature up to 80 °C. Therefore, the development of polymer electrolytes with high ionic conductivity has become one of the key subjects today in polymer science because of the potential application in electronic devices such as all solid-state rechargeable batteries or electrochromic windows [5]. Large research efforts have been

made to optimize the properties of polymer electrolytes, e.g., increasing the ambient ionic conductivity and improving the interfacial stability, to satisfy the needs of all solid-state lithium–polymer electrolyte batteries. Among the studies, introduction of inorganic fillers is one of the most successful ways. The addition of ceramic fillers, e.g., SiO_2, TiO_2, γ-$LiAlO_2$, or clay platelets, has increased the Li-ion transference number and improved the interfacial stability between the composite solid-state polymer electrolytes (CSPEs) and the lithium metal electrode [6–10]. The decrease in the filler size from micron scale to nanometer scale has increased significantly the surface-to-volume ratio and the conductivity [6, 11]. It is most interesting to point out that the introduction of molecular sieves [12–16] or the Lewis acid-type additives [17] into polymer matrix presented an efficient way to improve the conductivity and interface performance of polymer electrolytes.

It is known that the ionic conduction of the CSPEs depends strongly on the characteristics of filler particles, such as thermal history, surface area, porosity, size, and surface function groups [18–20]. In recent years, a new type of mesoporous molecular sieve, SBA-15, was synthesized [21]. This mesoporous material has a large specific surface area and highly ordered hexagonal arrangement of cylindrical mesopores, which account for the easy entrance and transference of ions or molecules in comparison with the microporous zeolite [22]. Because SBA-15 was synthesized by using triblock copolymers template, removal of the copolymers would lead to the development of irregular intrawall pores, which makes the material possesses a much larger specific surface area than common materials. SBA-15 holds larger pore diameter, thicker pore walls, and abundant surface groups –OH that makes the material stabilize and hydrophilic.

In this study, methyl group-functionalized mesoporous silica SBA-15 was synthesized and used as an inorganic filler in the preparation of the CSPE. The methyl group-functionalized SBA-15 powder exhibits hydrophobic pore surfaces, which are important to improve the miscibility between inorganic filler and inorganic matrix. The effects of the addition of surface functionalized SBA-15 on the conductivity; the crystalllinity and the morphology of the PEO_{10}–$LiClO_4$ system were studied systematically. Fourier transform infrared (FTIR) emission spectroscopy was employed for the first time to explore the temperature dependence of the transition of the PEO polymer matrix in CSPE from crystallization to the amorphous phase. Based on results of electrochemistry, scanning electron microscopy (SEM), and FTIR emission studies, the effect of inorganic filler on ionic conductivity and the electrochemical compatibility between the CSPE and a lithium metal electrode were revealed.

Experimental

Synthesis of methyl group-functionalized SBA-15

Mesoporous silica SBA-15 was synthesized following the procedure described in the literature [21] with slight modification. A triblock copolymer poly(ethylene oxide)–poly (propylene oxide)–poly(ethylene oxide), $EO_{20}PO_{70}EO_{20}$, was used as template for the preparation of mesoporous SBA-15 powder. First, 1.28 g of $EO_{20}PO_{70}EO_{20}$ was added to a beaker containing 50 ml 2 M HCl under stirring at ambient temperature until the triblock copolymer has completely dissolved. Then, 2.72 g of tetraethyl orthosilicate was added. The mixture was stirred at 40 °C for 24 h, transferred to a sealed container, and kept at 100 °C in an oven for 24 h. The resulting white precipitate was filtered and dried at 100 °C. Finally, the template was removed by calcination at 550 °C for 6 h to give fine mesoporous SBA-15 powder. SEM images show that the particle size of SBA-15 was ~1 μm. The average pore size and specific surface area of the calcined SBA-15, which were deduced from N_2 adsorption–desorption measurement, were respectively 6~7 nm and 652 $m^2\ g^{-1}$.

Calcined SBA-15 solid power was dried by heating under vacuum at 150 °C for 2 h and then functionalized with methyl groups. A sample of 1 g SBA-15 was introduced into 100 ml toluene containing 5 ml trimethylchlorosilane ($(CH_3)_3SiCl$) by stirring in a glove box filled with Ar for 6 h. The product was obtained by filtration, washed with toluene at least three times, dried by heating in vacuum at 120 °C, and then stored in the glove box filled with Ar. The resulting methyl group-functonalized SBA-15 is denoted as ^{f}SBA-15 thereafter. The alkyl chains $(–CH_3)_3$ attached to the SBA-15 are very short, making the ^{f}SBA-15 still retain the characteristic of parent SBA-15 concerning the average pore size and the specific surface area.

Preparation of composite solid-state polymer electrolyte

PEO (M_w~600,000, 99.98%, Aldrich) was dried at 50 °C, and $LiClO_4$ (from ACROS) and ^{f}SBA-15 were dried at 120 °C, respectively, for 24 h under vacuum before use. The given amounts of ^{f}SBA-15 and $LiClO_4$ were dispersed in anhydrous acetonitrile with ultrasound agitation for 15 min to form a mixture, and then the quantitative PEO powder was dissolved in the mixture by stirring. The mixture was cast on a Teflon dish with the approach of self-spread after 24 h of continuously stirring. The Teflon dish was placed into a desiccator to make acetonitrile absorbed by 4A zeolite at ambient temperature. The film obtained (about 110 μm in thickness) was dried in a vacuum oven at 65 °C for 2 days to remove the residual moisture. The

composition of the film is noted as PEO_{10}–$LiClO_4$/x% ^{f}SBA-15, in which the number of 10 in subscript gives the EO/Li ratio and the x% represents the weight percentage of ^{f}SBA-15 in PEO. The film thus formed is stored in a glove box filled with purified argon for further investigations.

Characterization and instruments

The composite solid polymer electrolyte was assembled into a cell of sandwich type. Three kinds of cell were assembled by this sandwich manner: (1) The film was sealed between two stainless steel (SS) electrodes (SS/CSPE/SS), (2) the film between a SS electrode and a lithium disk electrode (SS/CSPE/Li), and (3) the film between two lithium disk electrodes (Li/CSPE/Li). Ionic conductivity of CSPE was measured in the SS/CSPE/SS cell by AC impedance spectroscopy. The cells were kept at least 2 h in the temperature range of 30–90 °C, respectively, to reach the thermal equilibrium of the CSPE before the measurement. The frequency range was swept from 100 kHz to 1 Hz. Linear sweep voltammetry was used to test the electrochemical stability of the CSPE film in the SS/CSPE/Li cell. The measurements were done by slowly increasing the cell voltage until the onset potential of current to generate at 30 and 90 °C, respectively. The potential was swept from open circuit potential toward a more anodic potential at a scan rate 0.2 mV s^{-1}. The interfacial stability of the lithium electrode/solid-state polymer electrolyte was studied by comparing the impedance response of Li/CPSE/Li cell with or without filler at ambient temperature. The cell was stored under open circuit conditions, and the impedances were measured over a 100-kHz to 0.1-Hz frequency range. The above electrochemical experiments were carried out on an electrochemical workstation (CHI 660B, Chen-Hua, Shanghai, China). The AC perturbation signal was 5 mV. The obtained electrochemical impedance spectroscopy data were analyzed using the Z-view software.

Surface morphology of the composite electrolyte was inspected by using a scanning electron microscope (LEO 1530) with gold sputtering-coated films. X-ray diffraction (XRD) patterns, recorded in small angle and in wide angle as well, were recorded on an X'pert PRO (Japan) diffractometer. Thermal properties of the composite polymer membranes were studied by using a differential scanning calorimeter (DSC) (NETZSCH Thermal Analysis, DSC 204 cell, Netzsch Corp., German). The samples for the DSC test were placed in nonhermetic aluminum pans and then scanned from −100 to 200 °C at a heating rate of 20 °C min^{-1}. The melting enthalpy (ΔH_m) of the samples was obtained by integrating the endothermic peak of the DSC curves.

FTIR spectroscopic measurements were carried out on a FTIR spectrometer (Nicolet). FTIR spectra of SBA-15 powder and ^{f}SBA-15 powder were collected by thin flakes that were prepared by mixing the SBA-15 or ^{f}SBA-15 powder with KBr powder in the frequency range from 4,000 to 400 cm^{-1} using the AVATAR 370 FTIR spectrometer (Nicolet). FTIR emission experiments of the CSPE film were carried out on a Nexus 870 FTIR apparatus with liquid nitrogen-cooled mercury–cadmium–telluride detector. The CSPE film was prepared by coating composite polymer electrolyte solutions on Cu foils and then dried with the same procedures described in Section 2.2. The FTIR spectral resolution was 2 cm^{-1}.

Results and discussion

Structure and surface properties of methyl group-functionalized SBA-15

Figure 1 depicts the small-angle XRD pattern of SBA-15 and ^{f}SBA-15. Three well-resolved diffraction peaks that can be indexed respectively to the (100), (110), and (200) diffractions are observed in the region of 2θ=0.8–2° for the SBA-15. Such features represent characteristics of the long-range order of the hexagonal mesostructure. The three characteristic peaks can also be seen in XRD pattern of the ^{f}SBA-15, indicating that the long-range order of mesoporous hexagonal channels is still maintained. Furthermore, in comparison with XRD pattern of parent SBA-15, the three peaks of ^{f}SBA-15 are not shifted to high or low angle, implying that no contraction of framework of SBA-15 occurs after the methyl group functionalization. It may be inferred from above XRD results that the quantity of hydrophobic methyl group presented in the ^{f}SBA-15 is not enough to make a contraction of the framework of SBA-15. Function-

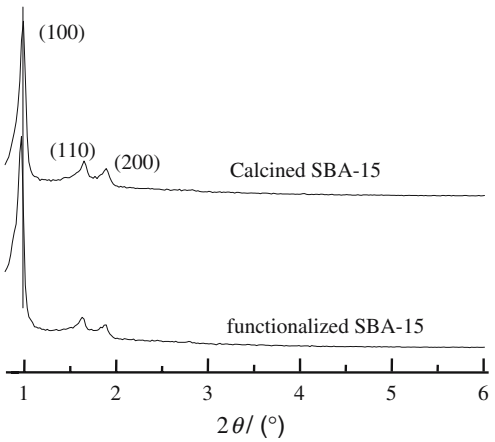

Fig. 1 Small-angle X-ray diffraction patterns of calcined SBA-15 power and ^{f}SBA-15 powder

alization changes the hydrophilicity/hydrophobicity of the surface in the SBA-15 and forms a hybrid mesoporous surface in ^{f}SBA-15 that increases not only the miscibility but also the mobility of PEO inside the ^{f}SBA-15.

The SBA-15 functionalized with methyl groups was investigated by FTIR spectroscopy. Figure 2 displays the FTIR spectra of powders of both SBA-15 and ^{f}SBA-15. Two new bands at 2,859 and 2,925 cm^{-1} appear in the spectrum of the ^{f}SBA-15 powder in comparison with that of SBA-15, which are assigned to infrared (IR) absorption of the symmetric and asymmetric C–H, respectively [23]. The presence of these IR bands indicates that the silanol groups (Si–OH) in SBA-15 have been replaced with methyl groups, which leads to the formation of a hydrophobic layer in the surface of SBA-15. Except for the IR bands of C–H, other IR bands are very similar in both spectra of SBA-15 and ^{f}SBA-15. Moreover, the intensity of the IR band near 3,430 cm^{-1} attributed to the silanol groups in the spectrum of SBA-15, and H_2O in atmosphere had not been weakened obviously, suggesting that only partial silanol groups have been replaced by methyl groups and the hydroxyl and methyl groups are coexistent in the external and internal surface of ^{f}SB-15.

Crystalline properties of solid-state polymer electrolyte films

DSC measurements are usually used to describe the effect of Li salt and inorganic filler on the thermal transition of the polyether side chain in polymer electrolytes. The melting enthalpy of materials can be determined by integrating the area under the DSC curve that is correlative with the crystallinity of the samples. The percentage of the crystalline PEO phase that is noted as crystallinity of PEO (χ_c) can be calculated by referencing to pure PEO being taken as 100% crystalline, i.e., a ratio of melting enthalpy of the PEO–LiClO4/x% ^{f}SBA-15 system to that of the pure PEO $\left(\chi_c = \Delta H_m / \Delta H_m^*\right)$. The values of glass transition temperature (T_g), melting temperature (T_m), and the χ_c of specimen including pure PEO, pure PEO film, and PEO–$LiClO_4$/x% ^{f}SBA-15 systems have been be obtained from DSC results and listed in Table 1. Along with the addition of the ^{f}SBA-15 filler, the T_m and χ_c of PEO in the PEO–$LiClO_4$/x%^{f}SBA-15 composite polymer electrolyte decrease obviously in comparison with those of the pure PEO film. When the content of the ^{f}SBA-15 filler is increased from 0 to 10 wt%, the χ_c is decreased acutely. While the content of ^{f}SBA-15 is increased from 10 to 15%, the χ_c is augmented from 26 to 53.27%. At the further increase in the content of ^{f}SBA-15 to 25%, the χ_c decreases again. We can see that the variation tendency of T_m of the film is the same as that of the χ_c. The decrease of the T_m and χ_c by addition of the ^{f}SBA-15 filler may proceed through two ways. In the one hand, the ether O atoms of PEO are bonded with the hydroxyl H atoms in free silanol of ^{f}SBA-15 (both external and internal surfaces) to form a transient cross-link that kinetically inhibits the ordered packing of PEO chains around the crystal seed that cause a relatively slack crystalline phase; on the other hand, PEO chains are intercalated into hybrid channels because of good miscibility between PEO and ^{f}SBA-15, which decreased the size of the crystalline PEO segment and increased the resistance of diffusion of PEO chain, as well as interrupted PEO segment movement, resulting in the decline of PEO crystallinity. When the silicon O atoms of ^{f}SBA-15 as the Lewis base are coordinated with Lewis acid lithium cations, both coordinated interactions were weakened between ether O atoms of PEO and Li^+ ions, as well as ether O atoms of PEO and hydroxyl H atoms in ^{f}SBA-15. The transient cross-link between the PEO chain and Li^+, as well as the PEO chain and ^{f}SBA-15, were released, resulting in an augment of

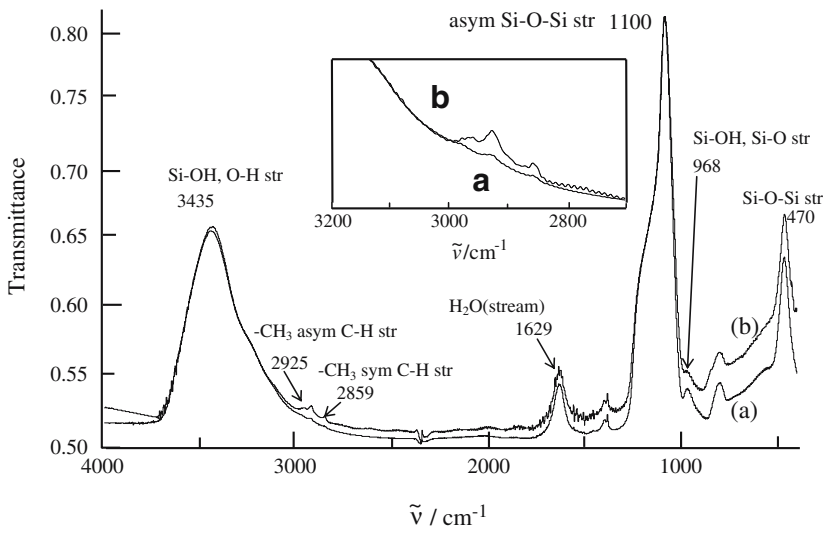

Fig. 2 FTIR spectra of **a** calcined SBA-15 powder and **b** ^{f}SBA-15 powder, and the types of vibrations involved are also indicated

Table 1 DSC data of pure PEO, pure PEO film. and PEO–$LiClO_4$/x% ^{f}SBA-15 systems

Sample	T_g (°C)	T_m (°C)	χ_c (%)
Pure PEO	–	73.1	100.0
Pure PEO film	–	75.4	80.5
PEO_{10}–$LiClO_4$/5%^{f}SBA-15	−36.4	60.9	41.5
PEO_{10}–$LiClO_4$/10%^{f}SBA-15	−30.1	60.6	26.0
PEO_{10}–$LiClO_4$/15%^{f}SBA-15	−34.3	64.4	53.3
PEO_{10}–$LiClO_4$/25%^{f}SBA-15	−35.3	60.6	41.5

PEO crystallinity, which may interpret reasonably the augmentation of T_m and PEO crystalline in 15% filler. The addition of the ^{f}SBA-15 filler leads to the contrary action for T_m and χ_c with the content of the ^{f}SBA-15 filler in the CSPE and produces a maximum of T_m and χ_c. In addition, there is no generally significant change in T_g (−30.1 to −36.4 °C) on the addition of the ^{f}SBA-15 filler, suggesting that the filler does not have an effect on the bulk property of PEO.

Figure 3 illustrates wide-angle XRD diffraction patterns of pure PEO, PEO_{10}/5% ^{f}SBA-15, and PEO_{10}–$LiClO_4$/x% ^{f}SBA-15, in which the variety of crystallinity of PEO with the content of the ^{f}SBA-15 filler can be qualitatively observed. Two primary characteristic diffraction peaks of crystalline PEO phase at 2θ=19 and 23.5° are observed from Fig. 3a. In comparison with XRD diffraction patterns of pure PEO (Fig. 3a), it can be found from Fig. 3b that two primary characteristic diffraction peaks of crystalline PEO decrease, which imply that the crystallinity of PEO decrease because of 5% ^{f}SBA-15 filler. Further, the diffraction peaks become weak and broad when the $LiClO_4$ and 5% ^{f}SBA-15 were added into the polymer matrix. The diffraction peaks of the crystalline PEO phase were still observable between 2θ=10 and 30°, illustrating that the PEO crystallinity is not be completely destroyed by the addition of $LiClO_4$ salt and ^{f}SBA-15 additive (from Fig. 3c to f). It is worthwhile to note that the intensity of diffraction peaks at 15% filler content is slightly higher than that at 10 and 25% filler in Fig. 3d,e,f, illustrating that silicon O atoms of ^{f}SBA-15 are competitively coordinated with Li^+. As a consequence, the coordination between ether O atoms of PEO and Li^+ and that between ether O atoms of PEO and hydroxyl H atoms in ^{f}SBA-15 are weakened. Such effect facilitates the ordered packing of PEO chains around the crystal seed and gives rise to high crystallinity. The result in Fig. 3e is also in accordance with the χ_c variation in DSC experiment.

SEM is usually used to survey the compatibility between the polymer matrix and filler. Figure 4 presents SEM images of pure PEO film, PEO_{10}–$LiClO_4$, and PEO_{10}–$LiClO_4$/x%^{f}SBA-15. The surface of pure PEO (Fig. 4a) is very smooth and shows the regular rumple, illustrating that there is a perfect crystallinity. The regular rumple is decreased and the surface looks rough in Fig. 4b, suggesting the reduction of PEO crystallinity. This can be explained by the coordination interaction between ether O atoms of PEO chain and lithium cations to form transient cross-links, which inhibit the reorganization of PEO chains effectively and hence decreases the recrystallization of PEO. We can see a smoother surface in Fig. 4c than that in Fig. 4b except for the regular rumple when 5%^{f}SBA-15 filler is added into polymer matrix. The rumple can be still seen but appear not regularly in Fig. 4d. Whereas the rumple in Fig. 4e began to appear more regular than that in Fig. 4d, it suggests that the PEO_{10}–$LiClO_4$/15%^{f}SBA-15 exhibits a higher crystalline than PEO_{10}–$LiClO_4$/10%^{f}SBA-15, being in consistent with the result of DSC and XRD. Moreover, phase separation between the polymer matrix and ^{f}SBA-15 filler are appeared in the case of the 25-wt% ^{f}SBA-15 filler (Fig. 4f). The SEM results demonstrated that hybrid ^{f}SBA-15 is highly dispersed in the polymer matrix to form a mechanically stable structure by the similar polarity at ambient temperature when the content of filler does not exceed 15%.

Electrochemical properties of CSPE films

Figure 5 shows the temperature dependence of ionic conductivity of filler-free PEO–$LiClO_4$ polymer electrolyte and those of PEO–$LiClO_4$/x% ^{f}SBA-15 polymer electrolyte (filler content from 5 to 25%) in a temperature region of from 30 to 90 °C. Among them, the polymer electrolyte at 5% ^{f}SBA-15 filler-loading content exhibits the highest ionic conductivity over a wide temperature range, especially below 70 °C (melting point of pure PEO). At 30 °C, the ionic conductivity of PEO–$LiClO_4$/5% ^{f}SBA-15 CSPE electrolytes is 3.26×10^{-6} S cm^{-1}, which is higher than that of PEO–$LiClO_4$ (1.38×10^{-7} S cm^{-1}) by more than one order of magnitude. The ionic conductivity of the CSPE

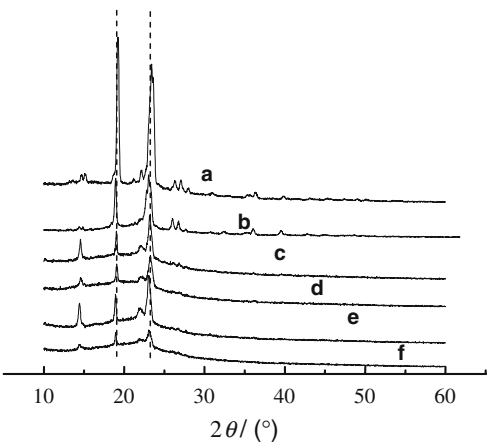

Fig. 3 Wide-angle X-ray diffraction patterns of pure PEO film (**a**), PEO_{10}/5%^{f}SBA-15 (**b**), PEO_{10}–$LiClO_4$/5%^{f}SBA-15 (**c**), PEO_{10}–$LiClO_4$/10%^{f}SBA-15 (**d**), PEO_{10}–$LiClO_4$/15%^{f}SBA-15 (**e**), and PEO_{10}–$LiClO_4$/25%^{f}SBA-15 (*f*)

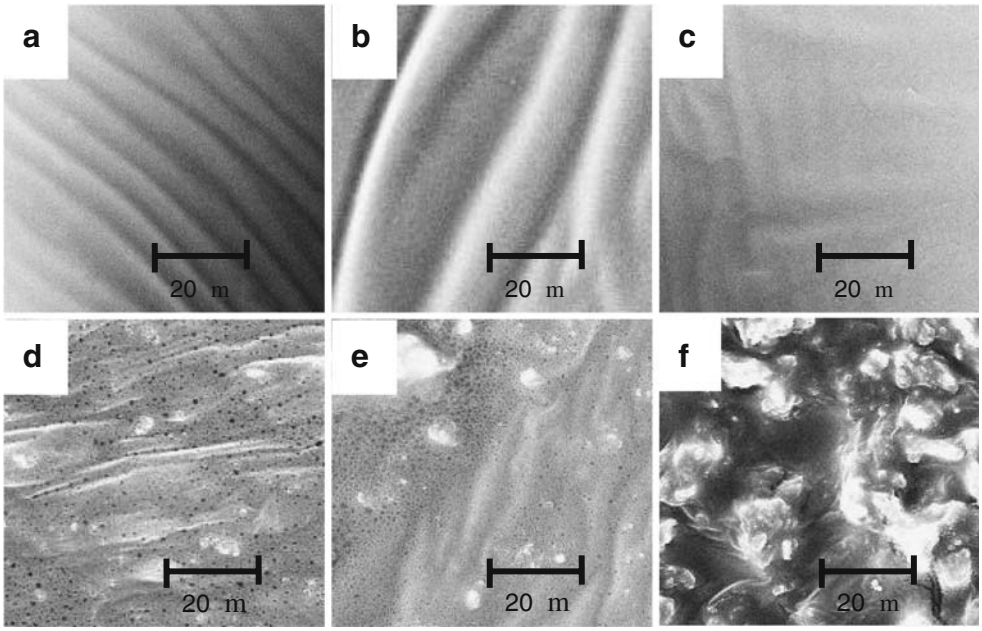

Fig. 4 SEM images of pure PEO film **a**, PEO_{10}–$LiClO_4$ **b**, and PEO_{10}–$LiClO_4$/x%^{f}SBA-15: **c** x=5; **d** x=10; **e** x=15; **f** x=25

film is decreased gradually when ^{f}SBA-15 concentration exceeds 5%. A significant decrease in the conductivity can be observed for PEO–$LiClO_4$/25% ^{f}SBA-15. The curve of the filler-free electrolyte shows a break point at 60 °C, and the ionic conductivity is increased linearly above the temperature. However, the curve is quite different for the PEO–$LiClO_4$/x% ^{f}SBA-15 polymer electrolyte, where the break point of the curve appears at around 50 °C. These results illustrated that the transition from crystalline state of PEO into the amorphous state begins from the break point that is about 10 °C lower than that of the melting point of specimen. Because PEO in PEO–$LiClO_4$ and PEO–$LiClO_4$/x% ^{f}SBA-15 mixtures exhibit a wide melting range, PEO has begun to be melting before the temperature rises to the melting point. A wide endothermic peak in the DSC curve of the PEO–$LiClO_4$ and PEO–LiClO4/x% ^{f}SBA-15 polymer electrolyte can verify the above analysis. The effect of the ^{f}SBA-15 additive on ionic conductivity may be attributed to additional ion-conducting pathways besides the cooperation interaction between ether O atoms of PEO and Li^+ cations. The additional ion-conducting pathways may be ascribed to the cooperation interaction between silicon O atoms of ^{f}SBA-15 and Li^+ cations, as well as to that the PEO is embedded into the hybrid channel of ^{f}SBA-15. The interactions of PEO, Li^+ cations, and ^{f}SBA-15 filler not only reduce the recrystallization tendency of PEO main chains but also provide additional Li^+ cations transmission route.

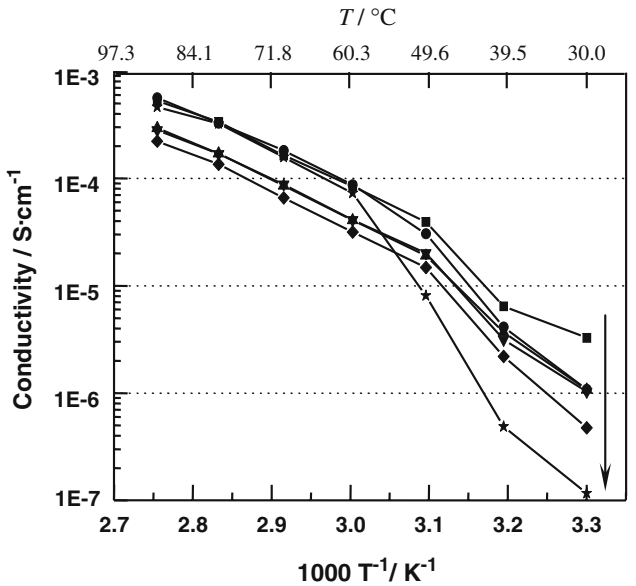

Fig. 5 Temperature dependence of ionic conductivity for PEO_{10}–$LiClO_4$/x% ^{f}SBA-15 composite polymer electrolyte, x is 5, 10, 15, 20, 25, and 0, respectively, from *top* to *bottom*

Table 2 lists the anodic electrochemical stable window of the PEO_{10}–$LiClO_4$ and composite polymer electrolytes PEO_{10}–$LiClO_4$/x% ^{f}SBA-15 films measured with SS/CSPE/Li cell at 30 and 90 °C, respectively. As it is well known, the onset potential of current flows in this type of

Table 2 Electrochemical stability windows of PEO_{10}–$LiClO_4$/x% ^{f}SBA-15 electrolytes containing different contents of ^{f}SBA-15 with SS/CSPE/Li cell

^{f}SBA-15 (wt%)	0	5	10	15	25
30 °C	4.81	5.16	5.53	5.31	5.12
90 °C	4.77	5.07	5.15	5.05	5.08

cell is associated with the decomposition potential of the given electrolyte. In the case of PEO_{10}–$LiClO_4$, the irreversible onset potential extends to about 4.8 V vs Li/Li^+, while the onset potentials of PEO_{10}–$LiClO_4$/*x*%^{f}SBA-15 films are all increased and exceeded 5 V vs Li/Li^+ at both temperatures. It is evident that the addition of ^{f}SBA-15 has substantially improved the stability of the electrolytes, leading the films to have wide electrochemical window and allow the use in an electrode system to the high voltage. Thus, they are suitable for the fabrication of the lithium batteries with high energy density [24].

It has been reported [15, 25] that 10% inorganic additive will give the optimal impact on CSPE. However, in the case of ^{f}SBA-15 filler, 5% yields the best performance in our system. As a comparison, Fig. 6 displays cyclic voltammograms of PEO_{10}–$LiClO_4$ and PEO_{10}–$LiClO_4$/10% ^{f}SBA-15 in a Li/CSPE/Li cell at ambient temperature. The CV results can be used for evaluating the electrochemical activity of the Li/CSPE interface. A pair of broad humps are observed in both the cathodic and anodic scans from Fig. 6a and b. The two electrodes system displays a high ohmic drop across the PEO_{10}–$LiClO_4$ and PEO_{10}–$LiClO_4$/10% ^{f}SBA-15 films because of the use of all solid polymer electrolytes and without a reference electrode in the electrochemical system. The efficiency of electron transfer passing the interface can be estimated by the peak-to-peak separation ΔE_p ($\Delta E_p = E_{pa} - E_{pc}$) and the broad humps current. In the case of PEO_{10}–$LiClO_4$, a pair of current peaks attributed to lithium dissolving (positive scan) and depositing (negative scan) appears at around 1.80 and −1.80 V, and the peak-to-peak separation ΔE_p is about 3.60 V. In the case of PEO_{10}–$LiClO_4$/10% ^{f}SBA-15, ΔE_p is about 2.80 V. The ΔE_p value is 0.80 V smaller than that of the PEO_{10}–$LiClO_4$, indicating

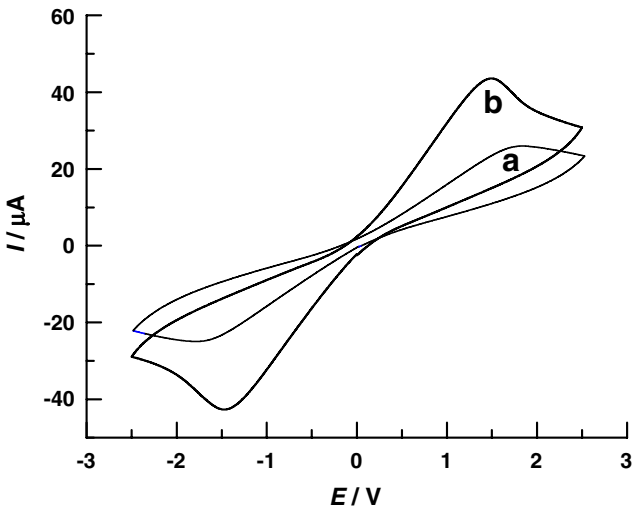

Fig. 6 Cyclic voltammograms of Li/CSPE/Li cell at 2 mV/s sweep rate at ambient temperature **a** PEO_{10}–$LiClO_4$ and **b** PEO_{10}–$LiClO_4$/10%^{f}SBA-15

that the interface of Li/PEO_{10}–$LiClO_4$/10% ^{f}SBA-15 has a better compatibility and electrochemical reversibility than those of Li/ PEO_{10}–$LiClO_4$ at ambient temperature [26]. In addition, the currents of anodic and cathodic peaks measured on Li/PEO_{10}–$LiClO_4$/10% ^{f}SBA-15 are much larger than those on Li/ PEO_{10}–$LiClO_4$, illustrating that the interface impedance is decreased and the capacity of charge and discharge is enlarged for the Li/PEO_{10}–$LiClO_4$/10% ^{f}SBA-15.

The passivation layer on the lithium electrode surface is a well-known phenomenon, which is the result of the corrosion between the metal lithium and the electrolyte. It is very important for cycling performance of the cell to obtain an improved interfacial property between lithium electrode and the CSPE. Impedance spectroscopy is a very convenient tool for monitoring interfacial phenomena. The time dependence of the interfacial resistance of PEO_{10}–$LiClO_4$ and PEO_{10}–$LiClO_4$/10% ^{f}SBA-15 in Li/CSPE/Li cells at ambient temperature is depicted in Fig. 7. The progressive expansion of the depressed semicircles is evidenced with time increasing. The depressed semicircles are associated with the passivation layer and the charge transfer resistance on the lithium electrode, which are considered to constitute the interfacial resistance (R_{int}) [26]. The interfacial resistance is increased rapidly, and the increase tendency is not uniform with time in the case of PEO–$LiClO_4$, while the interfacial resistance increases slowly and uniformly for the PEO_{10}–$LiClO_4$/10% ^{f}SBA-15 system. Moreover, the values of interfacial resistance of PEO_{10}–$LiClO_4$/10% ^{f}SBA-15/Li films are all smaller than those of PEO_{10}–$LiClO_4$/Li, demonstrating that the stability at interfaces has been improved when ^{f}SBA-15 filler is added to the PEO_{10}–$LiClO_4$ system. The addition of 10% ^{f}SBA-15 to the PEO–$LiClO_4$ electrolyte effectively slowed down the growth of the resistive layer on the lithium surface. By analyzing the impedance spectra, it may be suggested that the beneficial interfacial characteristics are based upon ^{f}SBA-15 with high surface area and similar polarity of ^{f}SBA-15 and PEO, which provide a good affinity to PEO matrix. The molecular sieves adsorbing trace water and impurities in the CSPE that prevents them from reacting at the interface is another complementary effect. As a consequence, it avoids that trace of corrosive residual solvents flow to the surface. Combining the above results with the SEM image of Fig. 4, we can see that the addition of 5% ^{f}SBA-15 filler presents an optimal interface compatibility with the polymer matrix.

Studies of the enhancement of ion conductivity of CSPE films by infrared emission spectroscopy

Figure 8a shows the FTIR transmission spectrum of pure PEO at ambient temperature, in which the triplet peak of the C–O–C stretching at about 1,144, 1,107, and

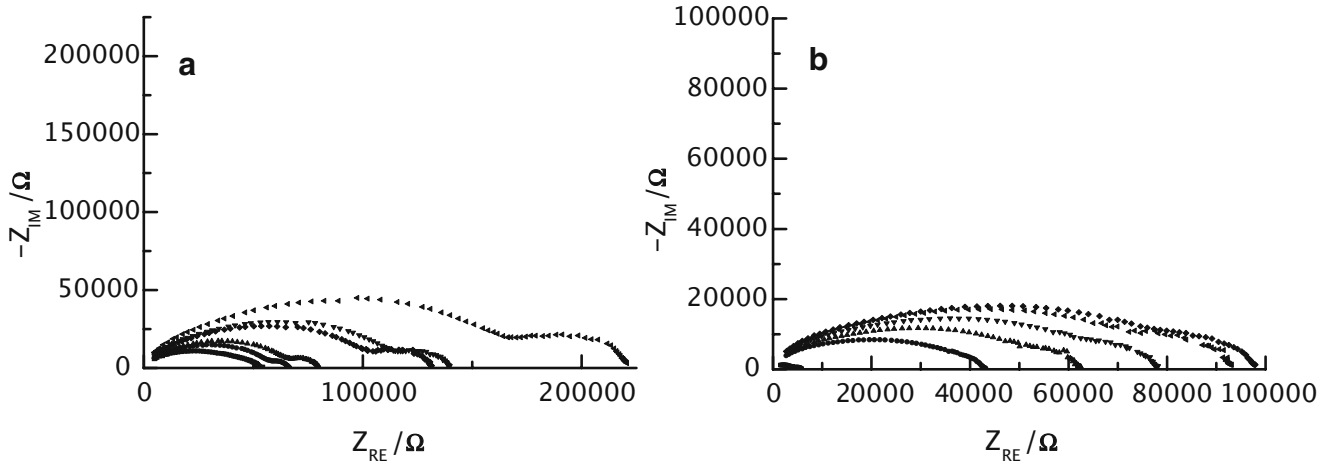

Fig. 7 Time dependence of the interfacial resistance at ambient temperature R_{int} in Li/CSPE/Li cells **a** PEO_{10}–$LiClO_4$, **b** PEO_{10}–$LiClO_4$/10%^{f}SBA-15. Li/CSPE/Li is put 0, 12, 48, 60, 96, and 120 h, respectively, from *inner* to *outer*

1,062 cm^{-1} and doublet peak of C–H wagging near 1,360 and 1,343 cm^{-1} are observed [27, 28]. The triplet peak around 1,100 cm^{-1} and the doublet peak close to 1,350 cm^{-1} can be usually used to confirm the presence of the crystalline PEO phase [27, 28]. FTIR emission spectroscopy was used to monitor the structure change of CSPE films with temperature. To investigate the relationship among ionic conductivity, temperature, and crystallinity of PEO, the temperature was varied within the same range as that in the measurements of ionic conductivity in Fig. 5. The temperature dependence of the FTIR emission spectra of PEO_{10}–$LiClO_4$ is shown from Fig. 8b to e. The doublet peak can be observed when temperature rises from 50 to 70 °C and is merged into a single peak progressively with further temperature rising. This variation in IR features illustrates that the amount of crystalline PEO is too small to be distinguished in spectra recorded above 70 °C. The temperature region is just coincided with the linear increase in ionic conductivity appearing in Fig. 5. Whereas for PEO_{10}–$LiClO_4$/5% ^{f}SBA-15 CSPE, only a single peak is observed near 1,350 cm^{-1} in all the FTIR emission spectra recorded in the whole temperature range from 50 to 100 °C (only 50 °C is presented in Fig. 8f). The above temperature dependence of emission FTIR results suggest that the recrystallinity of PEO is decreased, and the ratio of amorphous state of PEO is increased when only 5%^{f}SBA-15 is added into the PEO_{10}–$LiClO_4$ complex because the 5% ^{f}SBA-15 particles kinetically inhibit the ordered packing of PEO chains around the crystal seed to result in a relatively slack crystalline phase.

On the basis of the above data, the enhancement of ionic conductivity with the addition of 5% ^{f}SBA-15 filler may be analyzed. The Li^+ ionic conduction mechanism in a solid-state polymer electrolyte is still under discussion so far. It has been accepted widely [4] that the dominating type of Li ion transfer consists in that PEO chains coiled around the Li^+ cations, local relaxation, and segment motion of PEO chains make Li^+ transport in the PEO amorphous phase. The FTIR emission results above have demonstrated that the addition of 5%^{f}SBA-15 in polymer electrolyte has decreased recrystallization of PEO, which is responsible of high ionic conductivity. It has confirmed the mechanism, namely ion conducting through the PEO amorphous phase in the current system. In addition, the partial conductivity behaviors observed for the present system below T_m is based on Lewis acid–base interaction; for example, the oxygen atoms as Lewis base centers in both ^{f}SBA-15 filler and in PEO chains were combined with Li^+ cations for the formation of Li^+-containing complexes. The additional Lewis acid–base interactions have improved significantly the ionic conductivity of CSPE with the addition of the ^{f}SBA-15 filler, which is similar to that reported by Kao et

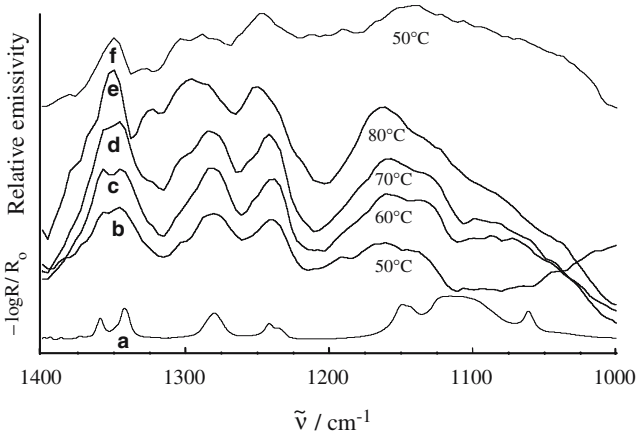

Fig. 8 **a** is FTIR transmission spectrum of pure PEO at room temperature, **b**, **c**, **d**, and **e** are temperature dependence of FTIR emission spectra of PEO_{10}–$LiClO_4$, and **f** is FTIR emission spectrum of PEO_{10}–$LiClO_4$/5%^{f}SBA-15

al. [16]. Moreover, SBA-15 exhibits large pore diameter, thick pore walls, and irregular intrawall pores. After having been modified by a methyl group, the ^{f}SBA-15 retains a large pore diameter (inferred from XRD spectrum [Fig. 1] and IR [Fig. 2]) and shows high miscibility with the PEO matrix because of similar polarity. The PEO chains may enter into the hybrid channel of ^{f}SBA-15, allowing that Li^{+} cations can get across the ^{f}SBA-15 mesoporous channels convoluted by PEO chains in the CSPE; that is, ^{f}SBA-15 provides more channels for Li^{+} cations transport.

Conclusion

In the current paper, we have prepared a novel methyl group-functionalized SBA-15 solid-state polymer electrolyte and studied the correlative properties with rechargeable lithium batteries. Temperature-dependence FTIR emission spectra were presented, for the first time, to elucidate the change of the crystallization degree of the polymer matrix with temperature and the inorganic additive. The results illustrated that FTIR emission spectroscopy is an indispensable tool to evaluate electrochemical properties of Li solid polymer electrolyte at various temperature. Studies of XRD, DSC, SEM, electrochemical impedance techniques, and FTIR emission spectroscopy demonstrated that the ^{f}SBA-15 additive in a PEO–$LiClO_4$ polymer electrolyte will facilitate salt dissociation, enhance ionic conductivity, and improve miscibility between the matrix and additive. Furthermore, the ionic conductivity depends on the ^{f}SBA-15 concentration, and the addition of 5–10 wt% of ^{f}SBA-15 in the PEO–$LiClO_4$ can enhance the ionic conductivity by more than one order of magnitude at 30 °C. The hydrophobic trimethylchlorosilane ($(CH_3)_3SiCl$) group on the surface of ^{f}SBA-15 plays an active role in affecting conductivity of the film, as it provides better specific surface interactions with the electrolyte components. It has revealed that the increase of Li^{+} ionic conductivity is based on two main approaches: (1) the Lewis acid–base interactions among the ^{f}SBA-15 surface, PEO chain, and lithium cations and (2) the ^{f}SBA-15 additive possesses high specific surface area, and the hybrid channel with 6–7- and 2–3-nm intrawall pores make more Li^{+} cations convoluted by hydrophobic PEO chains transport in it.

Acknowledgments This work was supported by National Key Basic Research and Development Program (Grant no. 2002CB211804) and Natural Science Foundation of China (Grants no. 20433040 and 20573085).

References

1. Tarascon JM, Armand M (2001) Nature 414:359
2. Fenton DE, Parker JM, Wright PV (1973) Polymer 14:589
3. Wright PV (1975) Br Polym J 7:319
4. Armand MB, Chabagno JM, Duclot JM (1979) In: Vashishta P, Shenoy JM, Shenoy GK (eds) Fast ion transport in solids. North Holland, New York, p 131
5. Gray FM (1991) Solid polymer electrolyte-fundamental and technological applications. VCH, New York
6. Croce F, Appetecchi GB, Persi L, Scrosati B (1998) Nature 394:456
7. Croce F, Curini R, Martinello A, Persi L, Ronci F, Scrosati B, Caminiti R (1999) J Phys Chem 103:10632
8. Vaia RA, Vasudevan S, Krawiec W, Scanlon LG, Giannelis EP (1995) Adv Mater 7:154
9. Sandi G, Carrado KA, Joachin H, Lu W, Prakash J (2003) J Power Sources 119:492
10. Chen HW, Chiu CY, Wu HD, Shen IW, Chang FC (2002) Polymer 43:5011
11. Krawiec W, Scanlon LGJ, Fellner JP, Vaia RA, Vasudevan S, Giannelis EP (1995) J Power Sources 54:310
12. Xi JY, Miao SJ, Tang XZ (2004) Macromolecules 37:8592
13. Xi JY, Ma XM, Cui MZ, Huang XB, Zheng Z, Tang XZ (2004) Chin Sci Bull 49:785
14. Xi JY, Li J, Tang XZ (2004) Acta Chimi Sin 62:1755
15. Xi J, Qiu X, Ma X, Cui M, Yang J, Tang X, Zhu W, Chen L (2005) Solid State Ion 176:1249
16. Kao HM, Tsai YY, Chao SW (2005) Solid State Ion 176:1261
17. Wieczorek W, Zalewska A, Raducha D, Florjanczyk Z, Stevens JR (1998) Phys Chem B 102:352
18. Choi B, Shin K (1996) Solid State Ion 86–88:303
19. Capuano F, Croce F, Scrosati B (1991) J Electrochem Soc 139:1918
20. Stevens JR, Wieczorek W (1996) Can J Chem 74:2106
21. Zhao D, Feng J, Huo Q, Melosh N, Fredrickson GH, Chmelka BF, Stucky GD (1998) Science 279:548
22. Jiang YX, Ding N, Sun SG (2004) J Electroanal Chem 563(1):15
23. Yang CT, Huang MH (2005) J Phys Chem B 109:17842
24. Appetecchi GB, Dautzenberg G, Scrosati B (1996) J Electrochem Soc 143:6
25. Reddy MJ, Chu PP (2004) J Power Sources 135:1
26. Nookala M, Kumar B, Rodrigues S (2002) J Power Sources 111:165
27. Li X, Hsu SL (1984) J Polym Sci Polym Phys Ed 22:1331
28. Bailey FE, Koleske JV Jr (1976) Poly (ethylene oxide). Academic, New York, p 115